Int J Thermophys (2015) 36:1784–1802
DOI 10.1007/s10765-015-1915-2

Traceability of a CCD-Camera System for High-Temperature Measurements

**L. Bünger[1] · K. Anhalt[1] · R. D. Taubert[1] ·
U. Krüger[2] · F. Schmidt[2]**

Received: 28 November 2013 / Accepted: 22 May 2015 / Published online: 27 June 2015

Abstract A CCD camera, which has been specially equipped with narrow-band interference filters in the visible spectral range for temperature measurements above 1200 K, was characterized with respect to its temperature response traceable to ITS-90 and with respect to absolute spectral radiance responsivity. The calibration traceable to ITS-90 was performed at a high-temperature blackbody source using a radiation thermometer as a transfer standard. Use of Planck's law and the absolute spectral radiance responsivity of the camera system allows the determination of the thermodynamic temperature. For the determination of the absolute spectral radiance responsivity, a monochromator-based setup with a supercontinuum white-light laser source was developed. The CCD-camera system was characterized with respect to the dark-signal-non-uniformity, the photo-response-non-uniformity, the non-linearity, and the size-of-source effect. The influence of these parameters on the calibration and measurement was evaluated and is considered for the uncertainty budget. The results of the two different calibration schemes for the investigated temperature range from 1200 K to 1800 K are in good agreement considering the expanded uncertainty ($k = 2$). The uncertainty for the absolute spectral responsivity of the camera is 0.56 % ($k = 2$).

Keywords Absolute spectral radiance responsivity · Charge-coupled device (CCD) · Dark-signal-non-uniformity (*DSNU*) · High temperature · Imaging radiometer · IRMD · Non-linearity (*NL*) · Photo-response-non-uniformity (*PRNU*) · Size-of-source effect (SSE) · Thermodynamic temperature

---

✉ L. Bünger
lars.buenger@ptb.de

[1] Physikalisch-Technische Bundesanstalt (PTB), Abbestraße 2-12, 10587 Berlin, Germany

[2] TechnoTeam Bildverarbeitung GmbH, 98693 Ilmenau, Germany

1 Introduction

Single-detector-element radiation thermometers are well established with respect to their technical setup and physical response, which allow a high quality calibration and measurements of radiometric quantities on the highest metrological level. Although CCD cameras are increasingly used on a research and industrial scale, the traceability of these instruments to the ITS-90 is yet not fully maintained and a standardized formalism to express the measurement uncertainties is not established. Compared to radiation thermometers, CCD cameras are superior in terms of being able to capture the temperature distribution over a two-dimensional area in just one reading, without the need for scanning over the scene of interest. Furthermore, CCD cameras allow a live view of the scene being measured. These advantages have made them as an ideal choice as monitoring devices, for example, in the detection of mechanical defects during manufacturing [1]. At the moment, their use in the field of precision thermometry is limited by the temperature calibration which is not offered as a standard service by NMIs and calibration laboratories. In order to increase the benefits of these instruments and to meet the user requirements, providing and maintaining traceability to the SI is of vital importance.

In principle, the established concepts for calibration and radiometric characterization [2,3] can be transferred also to the calibration of camera systems, yet additional effects have to be taken into account.

At first, it might seem that there are only small differences between single-detector-element radiation thermometers and CCD-camera systems. Both systems have, e.g., a detector, an optical lens system, spectral filters, and an electrical evaluation unit. However, the inhomogeneity of the optical system and filters has a significant influence on the signal levels over the detector area when using a CCD sensor. Instead of measuring a continuous photocurrent, CCD techniques are based on gathering electrons by discrete integration times.

As a first step to achieve a traceable calibration, a camera system with a fixed focus was exemplary characterized within this work. For the temperature calibration, a procedure similar to single-element-detector systems was developed. The photocurrent was replaced by an average value for a defined number of irradiated pixels. The investigated camera system is able to provide data either uncorrected as raw data from the internal analog-to-digital converter (*LSB*-mode) as well as corrected data (L-mode) with respect to, e.g., non-linearity (*NL*), shading.

2 CCD-Camera Characterization

The investigated CCD camera is a modified LMK 98-4 Color from the manufacturer TechnoTeam Bildverarbeitung GmbH. The camera is equipped with a six-position filter wheel unit. The standard configuration version uses four color filters and other additional filters such as scotopic luminance $V'(\lambda)$ filters [4]. Table 1 gives further details of the camera.

Table 1 Characteristics of the investigated camera system LMK-98 color (manufacturer information) [4]

Sensor	CCD Sony [ICX 285 AL (2/3″)]
Resolution	1380 × 1030 pixel
A/D conversion	12 bit
Integration time	100 µs … 15 s
Lens specification	
Measurement distance	800 mm, fixed focus length
Focal length	100 mm, fixed focal length
Aperture	Fixed aperture size
Measurement modes	*LSB*-A/D-converter count mode
	L-luminance mode
Repeatability	$\Delta L[<0.1\,\%]$
Uniformity	$\Delta L[<2\,\%]$
Internal selectable filter	Glass
	IF 450 nm
	IF 500 nm
	IF 650 nm
	IF 800 nm
	IF 900 nm
Analysis software	LMK LabSoft Standard Active X

IF interference filter

For temperature measurements above 1200 K, the CCD camera was specially equipped with narrow-band interference filters in the visible and near-infrared spectral ranges.

In the following section, relevant properties for the quasi "one-element-detector"-calibration will be discussed. These include the dark-signal-non-uniformity (*DSNU*), the photo-response-non-uniformity (*PRNU*), the non-linearity (*NL*) the *NL* with respect to the integration time and radiance level, and the size-of-source effect (SSE).

As described above, the camera can be used in two different modes. The LSB mode provides the uncorrected data from the internal analog-to-digital converter. Alternatively, the camera can be used in the so called L-mode; here the data are internally corrected for, e.g., the *PRNU* (f_{PRNU}), *NL* (f_{NL}), and *DSNU*. Other factors potentially considered for a correction such as the radiance calibration factor (k_{L}), the system transfer factor (k_{sys}), and the area factor (A_{p}) will not be discussed in this paper. These corrections and factors are implemented by the manufacturer into the camera software.

Equation 1 describes the model [5] for the determination of the L-values, which shall be proportional to the incoming radiance. These L-values (L) will be calculated automatically, by using the integration time (t_{int}), the uncorrected, measured *LSB* values (*LSB*), and the dark-signal (LSB_{DS}), which will be measured at the same time and conditions such as the *LSB* values of the irradiated pixel by using a permanently shadowed line of pixels located at the CCD margin.

$$L = \frac{1}{A_{\mathrm{P}}\, f_{\mathrm{PRNU}}} k_{\mathrm{L}} \frac{f_{\mathrm{NL}}\,(LSB - LSB_{\mathrm{DS}} - DSNU)}{k_{\mathrm{sys}} t_{\mathrm{int}}} \tag{1}$$

2.1 Dark-Signal-Non-uniformity (*DSNU*)

The *DSNU* describes the difference in dark signal between the pixels, in the form of a matrix for which each element of the matrix corresponds to a pixel of the matrix. The *DSNU* can be considered as a local scattering of the dark signal, whereby noise can be eliminated by averaging the individual pixel values using several images.

The *DSNU* was investigated with respect to ambient temperature and the integration time, while the camera was operated in a temperature-stabilized chamber. The objective lens was additionally covered by a lid to ensure only the dark signal was measured.

The temperature in the chamber was varied between 15 °C and 35 °C, and the signals of each pixel element were investigated for different integration times t_{int} in the range from 10 µs to 15 s. To suppress noise, the pixel element signals were averaged over 150 measurements for each ambient temperature and integration time setting. The repeatability of the dark signal and its distribution were investigated on different days. Figure 1 shows the difference in the dark signal along a horizontal line between two days and at an ambient temperature of 25 °C. The resulting repeatability is within an *LSB* value of ±0.5, e.g., for the pixels in the middle horizontal line (line number 520). This is less than one quantization step of the CCD A/D converter, and it seems to be stable and calculable. Especially for integration times larger than 1 s and high ambient temperatures above 31 °C, an increase of the pixel noise level in the *DSNU* images was observed.

In the *LSB* mode, a pixel value gradient perpendicular to the CCD registers of 3 % from the middle to the left side was recognized. This effect was probably caused by heat transfer from the electronic units at the left side of the CCD array, and a change

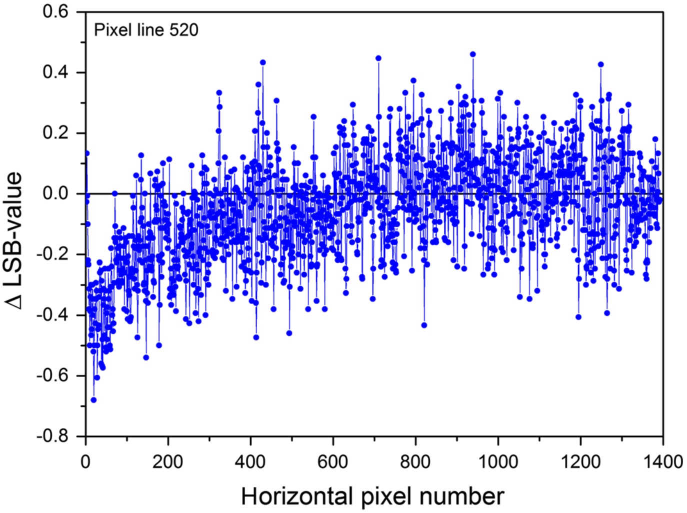

Fig. 1 Repeatability of the dark signal between two consecutive days for an ambient temperature of 25 °C and an integration time of 10^{-4} s. Dark-signal distribution in the LSB-mode is demonstrated for the central, *horizontal line* (line number 520) the CCD array

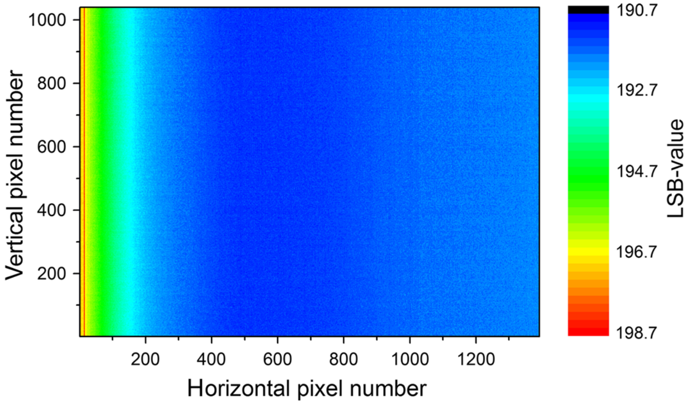

Fig. 2 Dark-signal-non-uniformity (*DSNU*) with underlying dark signal (DS) measured for an integration time of 10^{-3} s at an ambient temperature of 25 °C in the *LSB*-mode

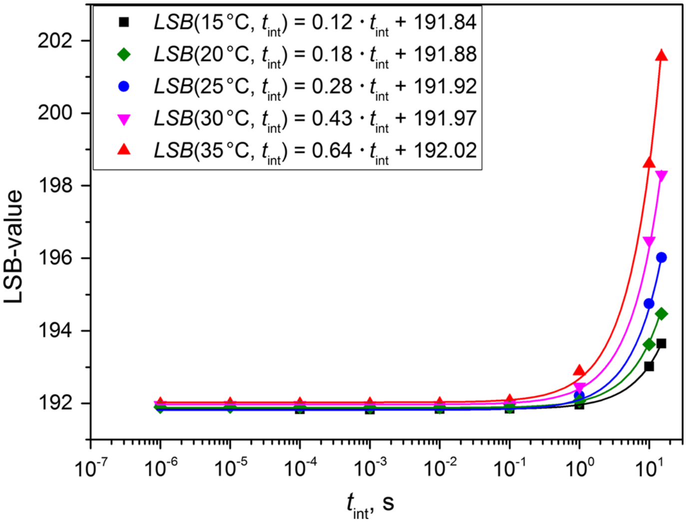

Fig. 3 Aproximation of the dark signal depending on the ambient temperature T_{amb} and the integration time t, by splitting the values into an integration time-dependent and -independent term

can be observed during the warm-up time of the camera system (Fig. 2). The mean LSB value of the dark-signal non-uniformity (including the gradient) with the underlying dark signal is 191.92 with a standard deviation of 1.12 measured with an integration time of 1 ms at an ambient temperature of 25 °C (Fig. 2).

The influence of the ambient temperature T_{amb} and integration time on the center area of the CCD array (average of 158 100 pixels corresponding to 11 % of all the pixels) is presented in Fig. 3. These measurement results can be approximated according to Eq. 2. The dark signal (LSB_{DS}) was split into an integration time-dependent term and an integration time-independent term. The integration time-dependent term can be understood as the genuine dark component (i.e., thermally generated electrons at the surface, bulk, or depletion region of the CCD) and the integration time-independent term originates from a bias introduced by the electronic components.

$$LSB_{\mathrm{DS}}\left(T_{\mathrm{amb}}, t\right) = a\left(T_{\mathrm{amb}}\right) \cdot t + b\left(T_{\mathrm{amb}}\right) \tag{2}$$

Equation 3 approximates a slightly linear dependence of the dark-signal values by changing the ambient temperature. Equation 4 describe the additional part, where this offset change varies exponentially with temperature T.

$$b\left(T_{\mathrm{amb}}\right) \approx 1034 \times 10^{-2}\,\mathrm{K}^{-1} T_{\mathrm{amb}} + 191.7 \tag{3}$$

$$a\left(T\right) \approx 0.025\mathrm{e}^{\left(0.0918\,\mathrm{K}^{-1} \cdot T\right)} \tag{4}$$

In case of the L-mode reading, these effects are compensated by the internal corrections. Therefore, no significant changes (with respect to the zero level in the signal) were observed.

2.2 Photo-Response-Non-uniformity (*PRNU*)

The *PRNU* describes variations in the responsivity between the pixels in the form of amplification factors. Usually the influence from the optical components dominates this characteristic, e.g., a radial distortion caused by the objective lens.

To investigate the *PRNU*, a source with a large and homogeneous illuminated aperture is required to take a flat-field image to normalize the images on a pixel-by-pixel basis. Here, an integrating sphere with an aperture diameter of 40 cm was used. For the field of view of the camera (approximately 53 mm × 40 mm), the inhomogeneity of the integrating sphere is less than 0.6 %. The long-term radiance stability was observed to be smaller than 0.2 % per hour and is additionally monitored by three photodiodes for drift correction purposes. Varying the radiance of the sphere without a significant change of the spectral distribution is possible by the use of shutters and/or switching off an increasing number of the 32 halogen-lamp pairs.

The camera was aligned to be centered to the circular axis of the integrating sphere at a focal distance of 800 mm between camera housing and the aperture of the integrating sphere. By changing the interference filter, the focal distance varies by a few millimeters. Because of the thickness of the filters, the internal mounting position, as well as the different inhomogeneities, individual correction matrices for each filter are used based on the normalized reciprocal values of the *PRNU* matrices.

Figure 4 displays the observed *PRNU* for the *LSB*-mode and the L-mode by using the 650 nm filter. The *PRNU* in the *LSB*-mode (non-corrected) shows the expected radial distortion which varies for the different interference filters by up to ±4 % (±4 K at 650 nm and $T = 1500$ K) with respect to the mean value. By using the L-mode (with internal correction), the observed variation is reduced to be less than ±1 % (±1 K at 650 nm and $T = 1500$ K), also depending on the used interference filter. Note, that for the temperature calibration of the camera (Sect. 3), only the 650 nm filter is used.

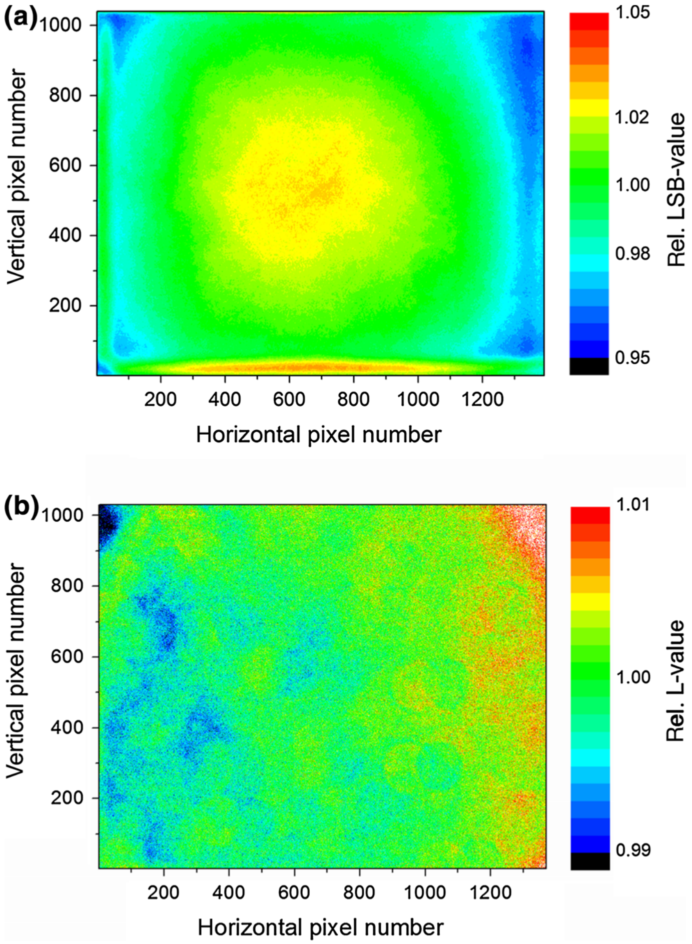

Fig. 4 Photo-response-non-uniformity (*PRNU*) of the camera (a) in *LSB*-mode and (b) in L-mode for a configuration with the 650 nm interference filter

2.3 Non-linearity (*NL*)

NL can be caused by the radiance level of the measured object and by the electronic parts, e.g., the signal amplifier [6,7].

In the case of a radiation thermometer, the *NL* describes a deviation from the proportional behavior between incident thermal radiation and the resulting output signal (e.g., photocurrent). For temperature measurements ($\lambda_c = 650\,\text{nm}$) in the range from 1200 K to 3200 K, a high dynamic range of about six orders in magnitude of the radiance/measuring signal is necessary and a measurement system should exhibit only a small *NL* to avoid increasing uncertainties due to corrections.

For a CCD-based imaging sensor system, a linear response over a wide range of radiance levels should be achieved. The pixels of a CCD array operate as capacitors using discrete integration times; therefore, the influence of the integration time on the *NL* has to be considered additionally. Finally, we have to distinguish between *NL* caused by the integration time ($NL(t,\ t_0)$) and *NL* caused by the incident flux ($NL(L)$).

The following equation offers the combined correction term $NL(L,\ t,\ t_0)$ for both *NL* contributions, which will be discussed in the next two subsections. $NL(L,\ t,\ t_0)$ is given as

$$NL\,(L, t, t_0) = NL\,(L) \cdot NL\,(t, t_0) \tag{5}$$

2.3.1 Non-linearity ($NL(t_{\mathrm{int}}, t_0)$)*: Integration Time Dependency*

The integration time-dependent non-linearity ($NL(t_{int}, t_0)$) was determined by varying the integration time t_{int} of the camera system while viewing a constant radiance output of the integrating sphere. The reference integration time t_0 was given by the highest possible signal without any overload of the A/D converter from the CCD array. The following equation describes the *NL* calculation for the *LSB* mode with LSB_{DS} as the corresponding dark signal:

$$NL\,(t_{\mathrm{int}}, t_0) = \frac{[LSB\,(t_{\mathrm{int}}) - LSB_{\mathrm{DS}}\,(t_{\mathrm{int}})]\,t_0}{[LSB\,(t_0) - LSB_{\mathrm{DS}}\,(t_0)]\,t_{\mathrm{int}}} \tag{6}$$

Equation 7 describes the *NL* calculation for the L-mode. With the internal corrections of the L-mode, the integration time is taken into account. Therefore, constant L-values for different integration times at a constant radiance level were expected. The signal at a CCD-charge level of 90 % ($L(t_{90\,\%})$) was used as the reference value:

$$NL\,(t, t_0) = \frac{L_{\mathrm{ph}}\,(t)}{L_{\mathrm{ph}}\,(t_{90\,\%})} \tag{7}$$

As a first measurement step, the maximum radiance setting of the integrating sphere was selected. The integration time was adjusted close to the critical overload of the A/D converter of the CCD array at 90 %. The integration time was subsequently reduced until the smallest integration time level was reached or the noise level dominated the signal. The same procedure was accomplished for different radiance settings.

The camera shows a non-linear characteristic, depending on the used interference filter (Fig. 5). Exemplary for the use of the 650 nm filter and very short integration times with just a few counts of the A/D-converter, a maximum deviation of 5 % is calculated for both measurement modes. By varying the integration time, the A/D converter level was found to be similar during the calibration and the measurements. For measurements with the same A/D-converter levels, this kind of *NL* is negligible. For other A/D-converter levels, a wavelength-dependent correction can be applied.

For further measurements with high dynamic levels, a *NL* correction is required. Alternatively, it is also possible to use different integration times to avoid this kind of *NL* correction for dynamic scenes.

2.3.2 Non-linearity (NL(L)): Radiance Level Dependency

The radiance-level-dependent *NL* was determined by using a *NL* measurement setup based on the flux-doubling technique [8].

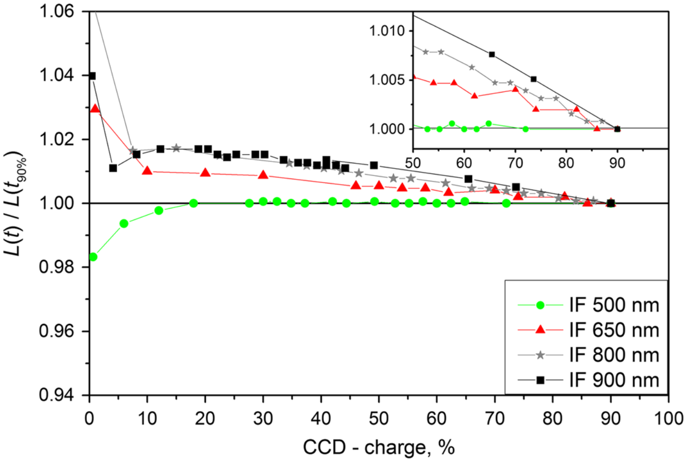

Fig. 5 Wavelength-dependent non-linearity ($NL(t)$) determined by varying the integration time t for a constant radiance field

A double aperture wheel, located in a parallelized beam part, is used to realize the different flux levels from 100 % ($L_{\mathrm{ph,A+B}}$) to 50 % and to 0 % for the dark-signal measurement. At the 100 % position, there is an open aperture with a centered vertical partition wall. At the 50 % positions, the right ($L_{\mathrm{ph,A}}$) or, respectively, the left side ($L_{\mathrm{ph,B}}$) is covered. The dark signal is measured with both partition openings covered ($L_{\mathrm{ph,DS}}$). The *NL* can be determined with:

$$NL\left(L_{\mathrm{ph,A+B}}\right) = \frac{L_{\mathrm{ph,A}} + L_{\mathrm{ph,B}}}{L_{\mathrm{ph,A+B}}} \tag{8}$$

An integrating sphere source with four halogen lamps ($P_{\mathrm{total}} = 200\,\mathrm{W}$) was used to realize high radiance levels and a large homogenous radiance field in order to irradiate the CCD array completely. For this investigation, the 650 nm interference filter was used. To cover the wide dynamic range of the camera, different neutral density absorption filters located in the beam path of the apparatus were used. To separate this kind of *NL* from the CCD-charge-depending *NL* (A/D converter level), the integration time for half flux was doubled.

The observed *NL* for the camera system is between 1.000 and 1.002 for values of L between 9 a.u. and 26 100 a.u. (Fig. 6). For values of L smaller than 9 a.u, a flux doubling method can no longer be used to investigate the *NL* as in this case, even the maximum integration time ($t_{\mathrm{int}} = 15\,\mathrm{s}$) would not suffice and the data would no longer be independent from the CCD-charge *NL*.

2.4 Size-of-Source Effect (SSE)

One of the reasons for the influence of the source size is scattered radiation incident on the detector; this effect is called the size-of-source effect or SSE [9,10]. The scattered radiation may originate from an area within or outside of the field of view. The SSE can

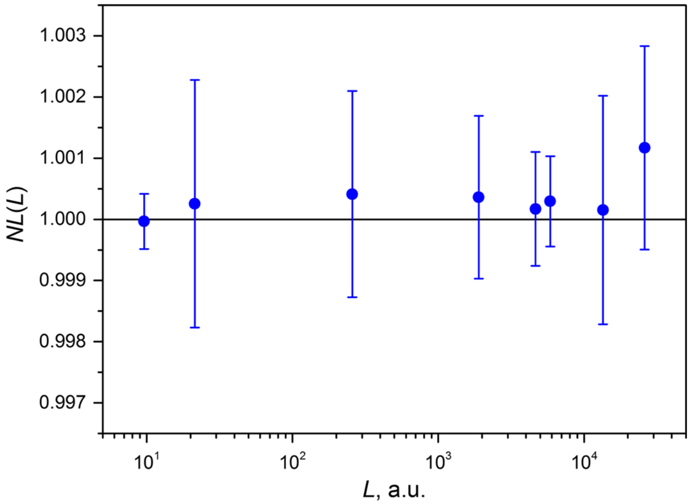

Fig. 6 Non-linearity depending on the radiance level ($NL(L)$) was determined by using a flux-doubling technique. An integrating sphere source was used to irradiate the complete CCD array with the 650 nm interference filter

be investigated by changing the size of a radiation source, e.g., by placing adjustable apertures in front of the radiation source, ensuring the output remains constant. For the determination of the size-of-source effect, the detection region was chosen smaller than the smallest aperture and the measuring field of the CCD array was not varied.

Studies were performed using the direct and the differential (indirect) methods to determine the SSE [11]. In the direct method, the aperture diameter d_a of a high-temperature blackbody was varied in the range from 3 mm up to 28 mm. Equation 9 describes the normalized SSE f_SSE with respect to the reference diameter d_ref of 5 mm, which was used for spectral calibrations. For both camera modes (LSB- and L-mode), the signals L_d were averaged for these investigations. The signals for the LSB mode are manually corrected with respect to the dark signal, while in the L-mode, it is automatically taken into account.

$$f_\mathrm{SSE}\left(d_\mathrm{a}, d_\mathrm{ref}\right) = \frac{L_\mathrm{d}\left(d_\mathrm{a}\right)}{L_\mathrm{d}\left(d_\mathrm{ref}\right)} \tag{9}$$

For larger apertures of up to 75 mm, a modified integrating sphere (LMT-LN3) was used. By changing defined apertures d_a and including an additional transparent plate with a black obscuration of diameter d_bb (reference plate), the size-of-source effect can be determined from the varying signal level at the obscuration for different aperture sizes [9]. Equation 10 describes the aperture-diameter-dependent coefficients σ_I by using the signal at the miniature blackbody ($L_\mathrm{bb}(d_\mathrm{bb})$) and the signal for the used aperture $L_\mathrm{d}(d_\mathrm{a})$. Equation 11 enables calculating the aperture-diameter-dependent values relative to the reference aperture diameter to generate a correction curve. This correction curve can be approximated with a polynomial function or spline interpolation function, because no point of discontinuity for this system is expected.

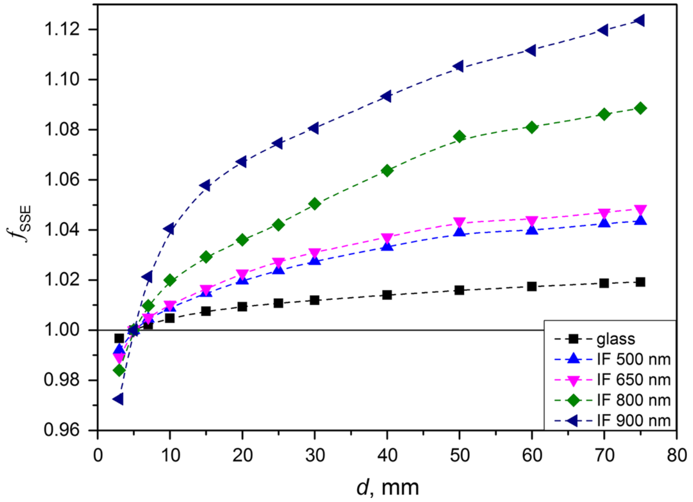

Fig. 7 Size-of-source effect (SSE) was determined at a modified integration sphere for the use of different interference filters according to the differential (indirect) method

$$\sigma_{\mathrm{I}}\left(d_{\mathrm{a}}, d_{\mathrm{bb}}\right)=\frac{L_{\mathrm{d}}\left(d_{\mathrm{a}}\right)-L_{\mathrm{bb}}\left(d_{\mathrm{bb}}\right)}{L_{\mathrm{d}}\left(d_{\mathrm{a}}\right)} \tag{10}$$

$$f_{\mathrm{SSE}}\left(\sigma_{\mathrm{I}}, \sigma_{\mathrm{I,ref}}\right)=\frac{\sigma_{\mathrm{I,ref}}}{\sigma_{\mathrm{I}}} \tag{11}$$

The relative uncertainty of the SSE correction was precautionarily estimated to be 25 %, based on not absolutely characterized aperture areas used to determine the size-of-source effect. Especially for small diameters, there is a high rate of change in the correction factor f_{SSE}. Additionally, the effective area of, e.g., high-temperature fixed-point cells has to be considered accurately to find a reliable SSE correction factor.

For the investigated camera system, a SSE of up to 12.3 % was observed (between $d_{\mathrm{ref}} = 5$ mm and $d_{\mathrm{a}} = 75$ mm) for the different interference filters, respectively, for the different wavelengths (Fig. 7). The results for the L-mode and the *LSB*-mode of the camera are consistent.

For high-temperature radiation thermometry applications in the range from 1200 K up to 3200 K, interference filters with center wavelengths close to 650 nm are usually used. For the 650 nm filter setup, a SSE of 4.8 %, corresponding to ±4.9 K at $T = 1500$ K, was determined for an aperture of 75 mm with respect to a reference aperture of 5 mm.

3 Temperature Calibration of the CCD Camera

Above the silver fixed point (1234.93 K), the international temperature scale of 1990 (ITS-90) is defined by a ratio measurement using Planck's law of thermal radiation and a temperature fixed point (either Ag, Au, or Cu) [12,13]. Alternatively, absolute radiometry offers to measure directly the thermodynamic temperature, if the absolute spectral radiance responsivity of a detector is well known [14].

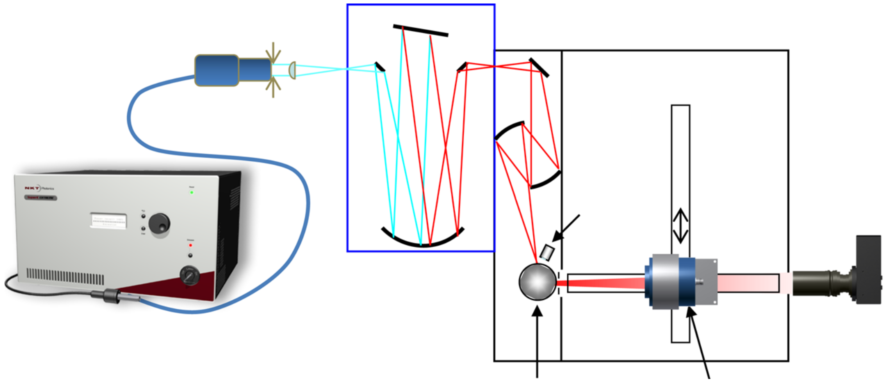

Fig. 8 Schematic of the PTB monochromator integrating-sphere-based spectral comparator facility

3.1 Experimental Setup and Procedures

For the absolute spectral radiance responsivity characterization of the camera, a monochromator integrating-sphere-based spectral comparator facility [3] was used (Fig. 8). Providing a homogeneous radiance field (integrating sphere), this facility allows calibration of the absolute spectral radiance responsivity of detector systems such as a radiation thermometer and also CCD cameras. Via a silicon photodiode trap detector as a transfer standard, the measurement is traceable to the PTB detector primary standard, the cryogenic radiometer. In order to maximize the radiance output of the integrating sphere, a supercontinuum laser system was used as a radiation source. By means of optical lenses and apertures, the laser beam was matched to the f-number of the monochromator system. The wavelength selection was performed by a monochromator system by using two different (precision) reflection gratings to cover the full spectral range of the silicon detector sensitivity. After the spectral selection, the radiation is focussed into an integrating sphere with an inner diameter of about 50 mm. The opening of this sphere toward the trap detector, respectively, the camera system is defined by a diamond-turned precision aperture with a nominal diameter of 5 mm. The traceability for the aperture diameter is given by a non-contact method [15].

This laser system was optimized with a dedicated controller to stabilize the radiance at the integrating sphere, which is equipped with a silicon photodiode. After a 15 min period of warm-up time for the laser system, the stabilization feedback realizes a high radiance stability with a variance of less than ±0.05 % per hour.

3.2 Determination of the Absolute Spectral Radiance Responsivity

The determination of the absolute spectral response is based on a spectral radiance responsivity measurement by a comparison with an absolutely calibrated trap detector. The geometric factor G (Eq. 12) is given by the radius of the precision aperture of the integrating sphere r_1, the precision aperture of the trap detector r_2, and the distance d between them [3].

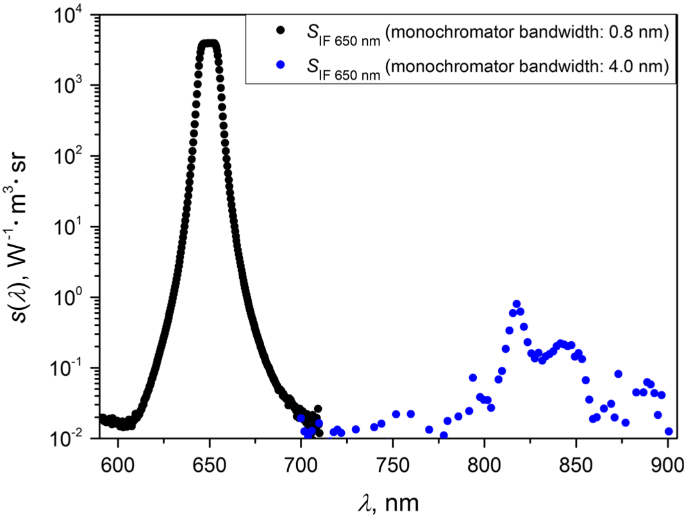

Fig. 9 Absolute spectral radiance responsivity of the investigated camera system with an interference filter at 650 nm (center wavelength: 649.74 nm ± 0.04 nm; bandwidth (*FWHM*): 10.72 nm ± 0.02 nm)

$$G(d, r_1, r_2) = \frac{2\pi r_1^2}{r_1^2 + r_2^2 + d^2 + \sqrt{\left(r_1^2 + r_2^2 + d^2\right)^2 - 4r_1^2 r_2^2}} \tag{12}$$

The following equation describes the calculation of the absolute spectral response of the camera system S^{L}_{LMK} by the geometric factor G, the aperture area A_2 of the trap detector, the signal of the camera L_{ph}, the photocurrent of the trap detector $I_{\mathrm{ph,Trap,}}$ the dark signal of the trap detector $I_{\mathrm{ph,Trap,DS}}$, and the spectral power responsivity S^{ϕ}_{Trap} of the trap detector:

$$S^{L}_{\mathrm{LMK}}\left(\lambda, d, r_1, r_2\right) = G(d, r_1, r_2)\frac{L_{\mathrm{ph}}}{I_{\mathrm{ph,Trap}} - I_{\mathrm{ph,Trap,DS}}} A_2 S^{\phi}_{\mathrm{Trap}}\left(\lambda\right) \tag{13}$$

The dark signal in the used L-mode is automatically determined and internally taken into account. The band-pass region from 590 nm up to 710 nm was investigated with an effective monochromator bandwidth of 0.8 nm and a step size of 0.4 nm by using a grating with 1302 lines per mm. The measured L_{ph} values (in arbitrary units, a.u.) vary over five decades before the noise dominates the signal. For the spectral range from 700 nm up to 900 nm, a grating with 651 lines per mm was used. For this setup, the usable spectral power of the laser system in combination with the monochromator decreases by a factor of 10. For the out-of-band region, a spectral bandwidth of 4 nm and a step size of 2 nm were used. Between 800 nm and 900 nm, the spectral radiance responsivity increases slightly to a value of 1 W^{-1}·m^{3}·sr, compared to the maximum of around 3500 W^{-1}·m^{3}·sr in the bandpass region (Fig. 9). For temperature measurements, the out-of-band structure in the near-infrared region has to be taken into account. Due to the spectral distribution of Planck's law, this out-of-band responsivity generates up to 2 % of the measurement signal at low temperatures and this ratio decreases with increasing temperatures.

To achieve a good signal-to-noise ratio for every wavelength setting, the integration time of the camera was varied from 0.2 s for the bandpass region up to 15 s for the out-of-band region.

For the spectral calibration, measured signals were averaged over 5810 pixels in a central region. The center wavelength was determined to be (649.74 ± 0.04) nm with a full width at half maximum (*FWHM*) of (10.72 ± 0.02) nm.

With this spectral radiance responsivity calibration, the thermodynamic temperature of, e.g., a blackbody can be calculated iteratively (Eq. 14) using the emissivity $\varepsilon(\lambda)$ and Planck's law of thermal radiation with the first radiation constant $c_1 = 2\pi hc^2$, second radiation constant $c_2 = hck^{-1}$, Planck's constant h, Boltzmann's constant k, and the speed of light c.

$$L_{\mathrm{ph,LMK}} = \int \varepsilon(\lambda) \frac{c_1}{\pi \lambda^5} \frac{1}{\mathrm{e}^{\frac{c_2}{\lambda T}} - 1} S^L_{\mathrm{LMK}} \mathrm{d}\lambda \tag{14}$$

Alternatively, the blackbody temperature can be determined traceable to the international temperature scale ITS-90 using a calibrated radiation thermometer as shown in Sect. 3.3.

3.3 Determination of the Temperature Response with Respect to ITS-90

In order to validate the absolute spectral radiance responsivity calibration of Sect. 3.2, the camera was used to measure the temperature of the high-temperature blackbody radiator HTBB3200pg.

Comparing the results of the different temperature measurements allowed the validation of the spectral radiance responsivity measurement and also the development of a calibration scheme for the camera systems in terms of the ITS-90.

The camera was aligned concentrically and focused to the aperture area of the blackbody radiator. The temperature of the blackbody was varied in the range from 1200 K to 2000 K. The ITS-90 temperature of the blackbody radiator was determined by an ITS-90 calibrated radiation thermometer LP3 (manufacturer: KE Technologie GmbH) before and after the camera measurements to cover possible temperature drifts. For this calibration, half of the blackbody's aperture area was evaluated, and the measured signals were averaged over 158100 pixels. The integration time varied between 0.2 ms and 25 ms for the given temperatures. For temperatures above 1900 K, an additional neutral density filter had to be used and therefore, e.g., *PRNU* matrices had to be estimated. The following equation [16,17] allows determination of the coefficients a, b, and c by least-squares fitting:

$$T_{90}\left(L, a, b, c\right) = \frac{1}{a}\left(\frac{0.014388}{\ln\left(\frac{c}{L} + 1\right)} - b\right) \tag{15}$$

as a function of the temperature $T_{90}(L, a, b, c)$. The residuum of the fit using the 650 nm filter is specified to be ±0.2 K for the L-mode and ±0.3 K for the *LSB*-mode

Table 2 Fit function parameters

	L-mode[a]	*LSB*-mode[b]
a (m)	$6.43734 \times 10^{-7} \pm 0.05664 \times 10^{-7}$	$6.47322 \times 10^{-7} \pm 0.06730 \times 10^{-7}$
b (K·m^{-1})	$2.70539 \times 10^{-6} \pm 4.27190 \times 10^{-6}$	$0.80305 \times 10^{-6} \pm 5.09186 \times 10^{-6}$
c (A)	$5.29521 \times 10^{10} \pm 0.33727 \times 10^{10}$	$2.01990 \times 10^{12} \pm 0.15128 \times 10^{12}$
Effective wavelength (nm)	645.2 ± 8.0	647.8 ± 9.5
Max. residuum	±0.2 K	±0.3 K
Temperature range	1250 K to 1780 K	1250 K to 1780 K

[a] Camera measurement mode with internal corrections (L-mode)

[b] Camera measurement mode with the raw uncorrected data from the analog-to-digital converter (LSB-mode)

($1250\,\mathrm{K} < T < 1780\,\mathrm{K}$). Table 2 shows the determined coefficients for the used 650 nm filter for both modes.

The following equation gives the temperature-dependent (extended) effective wavelength λ_x which is well approximated by a linear function of inverse temperature with the coefficients a and b from Eq. 15 [18]:

$$\lambda_x = a + \frac{b}{T} \tag{16}$$

The extended effective wavelengths are 645.09 nm (1200 K) and 645.99 nm (2000 K) for the L-mode, and 647.77 nm at 1200 K and 647.99 nm at 2000 K for the *LSB*-mode.

3.4 Uncertainty Budget

The relevant uncertainty components for the calibration at the monochromator integrating-sphere-based spectral comparator facility are presented in Table 3. A major contribution is given by the non-uniformity of the integrating sphere. Increasing the inner diameter of the integrating sphere improves the radiance homogeneity in the aperture area, but the radiance will decrease. For detector systems with a larger field of view and also for camera systems, a relatively large aperture in front of the integrating sphere is preferable. However, for an integrating sphere with a given inner diameter, the homogeneity will decrease and thus the measurement uncertainty will increase with increasing aperture sizes. A good compromise between spatial homogeneity and achievable radiance level was found by using a 5 mm aperture in conjunction with an integrating sphere with an inner diameter of 50 mm.

The stability of the spectral radiance is directly measured at the entrance opening of the integrating sphere by a photodiode. For the used spectral bandwidths of 0.8 nm and 4 nm, the spectral radiance stability was better than 0.1 % per hour. The distance between the apertures was measured with a calibrated length gauge with a relative accuracy of 0.05 %.

The temperature responsivity was determined with respect to the ITS-90 at a blackbody radiator with a standard radiation thermometer as the reference (type: LP3). The

Table 3 Summary of relative uncertainty contributions for the calibration of the absolute spectral responsivity measurement facility [3]

Quantity	Contributions of uncertainty	Relative uncertainty (%) ($k = 1$)
u_1	Spatial homogeneity int. sphere	0.16
u_2	Source instability	0.05
u_3	Repeatability	0.05
u_4	Spectral responsivity of the trap	0.03
u_5	Aperture area	0.02
u_6	Distance	0.05
u_7	Diffraction at two apertures	0.05
u_8	Effective wavelength	0.05
u_9	Bandwidth effect	0.04
u_{10}	Stray light effect	0.01
u_{11}	Photo-response-non-uniformity	0.20
$u(k = 1)$	Total uncertainty, root sum squared	0.28

spatial homogeneity and the temperature accuracy of the radiator dominate the uncertainty budget for this calibration method with a contribution of 0.5 K. The stability of the blackbody radiation amounts to 0.2 K.

The uncertainty components discussed above are not specific for camera calibrations and would be valid for the calibration of single-element detectors such as radiation thermometers or filter radiometers as well. Additional uncertainty components are connected specifically for two-dimensional measurement systems. The stated uncertainties are considered for the irradiated region of the CCD array. In both calibration schemes, the pixel signals over a defined region were averaged and the pixel-to-pixel variation is taken into account. Therefore, groups of pixels can be used for a traceable temperature determination within the given uncertainty.

For other regions or a field of view of different size, the *PRNU* is considered to contribute 1 % (±1 K at 650 nm and $T = 1500$ K) to the uncertainty budget. The uncertainty associated with the SSE correction is assumed to be 25 % of this correction (Sect. 2.4).

3.5 Results

The camera was calibrated with respect to its absolute spectral radiance responsivity and with respect to the temperature response of a high-temperature blackbody radiator, according to the ITS-90. The difference between the radiometrically determined thermodynamic temperature and the ITS-90 temperature was determined iteratively for the measured L-values at the blackbody radiator. In Fig. 10 the temperature differences of the calibrations are shown. For the two measurement schemes, the size of the radiating source differs. The diameter of the integrating sphere aperture for the absolute spectral calibration was 5 mm, while the diameter of the blackbody aperture

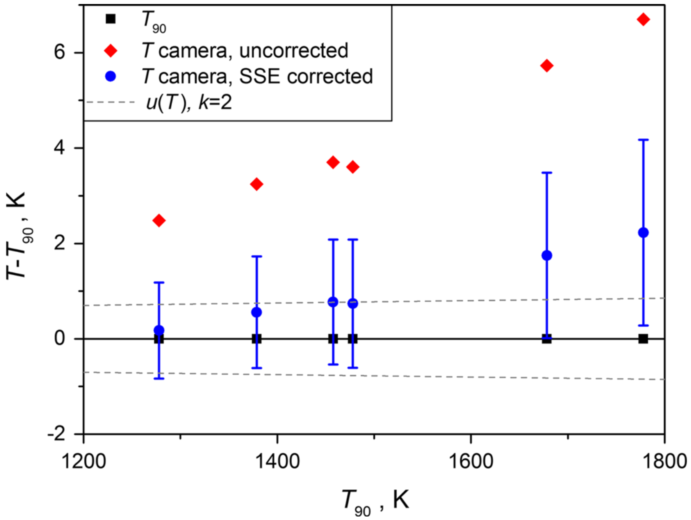

Fig. 10 Comparison of the absolute spectral radiance responsivity calibration with the ITS-90 traceable blackbody calibration

was 28 mm (Fig. 7). Therefore, a correction of the SSE with a factor of $f_{\mathrm{SSE}} = 1.032$ was carried out. The signal level for high-temperatures measurements in the range from 1200 K up to 1800 K differs by up to 7 K at 1777.9 K for uncorrected values. The SSE correction reduced this maximum deviation to 2.2 K. The results were not corrected with respect to *NL* because of similar A/D-converter counts for both calibrations, yet the integration times were different. The presented results show good agreement considering the expanded uncertainty ($k = 2$).

4 Conclusions

A special version of the camera system “LMK 98-4 Color” allows measurements of temperatures in the range from 1200 K up to 1800 K. For measurements of higher temperatures, an additional neutral density filter has to be used.

Two schemes for a temperature calibration of the camera’s L-mode (i.e., with internal corrections for *NL, PRNU, DSNU*) were investigated. In the following, the main findings are summarized for the observed signal variation with respect to temperature variation.

The dark signal and its distribution will be compensated by internal corrections, so no significant changes of the zero level in the signals were observed. *NL* takes effect when measuring high dynamic scenes, due to different signal levels of the A/D converter. When measuring over a dynamic scene, a nonlinear behavior was observed, and found to be dependent on the spectral range. The maximum deviation caused by *NL* for the 650 nm interference filter and A/D-converter levels between 5 % up to 90 % is on the order of 2 % (±2 K at 650 nm and $T = 1500$ K). However, for a moderate range of 50 % up to 90 % of A/D-converter level, the difference is less than 0.5 % (±0.5 K at 650 nm and $T = 1500$ K).

Using a reference radiation thermometer, the camera system was calibrated traceable to ITS-90. In this case, a potential *NL* of the detector system is in large part implemented in the calibration scheme for homogeneous radiance fields and adequate integration times for comparable A/D-converter levels. Even for an exact fitting, the error caused by *NL* would be zero at the calibration points and non-zero between them. For least-squares fitting, the error is always non-zero but is partially taken into account in the fitting process [19]. A correction of the *PRNU* can be more difficult, depending on the used filter and its exact positioning in the mechanical optical system. However, by the use of the camera system over the same region as calibrated, the *PRNU* does not have to be additionally taken into account. Nevertheless, when other areas of the CCD array are used during a measurement, the effect of the *PRNU* was found to be on the order of 1 % (±1 K at 650 nm and $T = 1500\,\mathrm{K}$).

The SSE dominates the uncertainty budget depending on the calibration conditions and the use of the camera at the blackbody. For the described calibration methods, a SSE correction is necessary if the diameter of the radiating sources differ. The diameter of the integrating sphere aperture for the absolute spectral calibration was 5 mm, while the diameter of the blackbody aperture was 28 mm. In this case, the signal of the absolute spectral calibration has to be corrected by the factor $f_{\mathrm{SSE}} = 1.032$. The uncertainty is assumed to 25 % of the correction factor. For larger apertures, a size-of-source effect of up to 6 % (±6 K at 650 nm and $T = 1500\,\mathrm{K}$) was observed.

The camera was calibrated with respect to its absolute spectral radiance responsivity and its response to temperature radiation traceable to the ITS-90 using a high-temperate blackbody radiator. The temperature deviations between the thermodynamic temperature T and the ITS-90 temperature T_{90} were determined iteratively for the measured L-values at the blackbody radiator. The temperature deviation at high temperatures for measurements in the range from 1200 K up to 1800 K differs by up to 6.5 K at 1777.9 K for uncorrected values, and by up to 2 K with a recommended SSE correction. An *NL* correction was not performed due to similar A/D-converter counts for both calibrations.

This presented work demonstrates the ability to calibrate camera systems according to its absolute spectral radiance responsivity as well as to the ITS-90. By comparing these two different calibration schemes, different contributions to the measurement uncertainty relevant for calibration and later application were evaluated.

Acknowledgment This work was funded by the German Federal Ministry of Economics and Technology (BMWi) in the framework of the MNPQ programme.

References

1. P. Saunders, T. Ricolfi, in *Proceedings of TEMPMEKO '96, 6thInternational Symposium on Temperature and Thermal Measurements in Industry and Science*, ed. by P. Marcarino (Levrotto and Bella, Torino, 1997), pp. 329–334
2. Mise en pratique for the definition of the Kelvin, http://www.bipm.org/utils/en/pdf/MeP_K.pdf
3. T. Keawprasert, K. Anhalt, D.R. Taubert, J. Hartmann, Int. J. Thermophys. **32**, 1697 (2011)
4. http://www.technoteam.de/product_overview/lmk/index_eng.html. Accessed 3 July 2014
5. U. Krüger, F. Schmidt, Metrologia **46**, S252 (2009)
6. H.E. Bennett, Appl. Opt. **5**, 1265 (1966)

7. J.R. Janesick, *Scientific Charge-Coupled Devices* (SPIE, Bellingham, 2001)
8. H.J. Jung, Metrologia **15**, 173 (1979)
9. P. Bloembergen, Metrologia **46**, 534 (2009)
10. P. Saunders, Int. J. Thermophys. **32**, 1633 (2011)
11. P. Saunders, H. Edgar, Metrologia **46**, 62 (2009)
12. H. Preston-Thomas, Metrologia **27**, 3 (1990)
13. H. Yoon, P. Saunders, G. Machin, in *Supplementary Information for the ITS-90: Section 6: Radiation Thermometry*, pp. 1–13. http://www.bipm.org/en/publications/its-90_supplementary.html. Accessed 19 Mar 2015
14. J. Fischer, M. de Podesta, K.D. Hill, M. Moldover, L. Pitre, R. Rusby, P. Steur, O. Tamura, R. White, L. Wolber, Int. J. Thermophys. **32**, 12 (2011)
15. J. Hartmann, J. Fischer, J. Seidel, Metrologia **37**, 637 (2000)
16. H. Jung, J. Verch, Optik **38**, 95 (1973)
17. F. Sakuma, S. Hattori, *Temperature, Its Measurement and Control in Science and Industry*, vol. 5, ed. by J.F. Schooley (AIP, New York, 1982), pp. 421–427
18. G. Machin, P. Bloembergen, K. Anhalt, J. Hartmann, M. Sadli, P. Saunders, E. Woolliams, Y. Yamada, H.W. Yoon, *Realisation and Dissemination of Thermodynamic Temperature Above the Silver Point (1234.93 K), CCT-WG5 Document, CCT-10/12/rev1* (BIPM, Sèvres, 2010)
19. P. Saunders, Metrologia **40**, 93 (2003)